



Ocean Heat Uptake in Transient Climate Change: Mechanisms and Uncertainty due to Subgrid-Scale Eddy Mixing

BOYIN HUANG, PETER H. STONE, AND ANDREI P. SOKOLOV

Joint Program on the Science and Policy of Global Change, Massachusetts Institute of Technology, Cambridge, Massachusetts

IGOR V. KAMENKOVICH

Department of Atmospheric Sciences, University of Washington, Seattle, Washington

(Manuscript received 30 January 2003, in final form 20 April 2003)

ABSTRACT

The ocean heat uptake (OHU) is studied using the Massachusetts Institute of Technology (MIT) ocean general circulation model (OGCM) with idealized ocean geometry. The OGCM is coupled with a statistical–dynamic atmospheric model. The simulation of OHU in the coupled model is consistent with other coupled ocean–atmosphere GCMs in a transient climate change when CO₂ concentration increases by 1% yr⁻¹. The global average surface air temperature increases by 1.7°C at the time of CO₂ concentration doubling (year 70). The ocean temperature increases by about 1.0°C near the surface, 0.1°C at 1000 m in the Pacific, and 0.3°C in the Atlantic. The maximum overturning circulation (MOTC) in the Atlantic at 1350 m decreases by about 4.5 Sv (1 Sv ≡ 10⁶ m³ s⁻¹). The center of MOTC drifts upward about 300 m, and therefore a large OTC anomaly (14 Sv) is found at 2700 m. The MOTC recovers gradually, but the OTC anomaly at 2700 m does not seem to recover after CO₂ concentration is kept constant during 400-yr simulation period.

The diagnosis of heat flux convergence anomaly indicates that the warming in the lower latitudes of the Atlantic is associated with large-scale advection. But, the warming in the higher latitudes is associated with the heat brought down from the surface by convection and eddy mixing. In global average, the treatments of convection and eddy mixing are the two main factors affecting the OHU.

The uncertainty of OHU due to subgrid-scale eddy mixing is studied. In the MIT OGCM this mixing is a combination of Gent–McWilliams bolus advection and Redi isopycnal diffusion (GMR), with a single diffusivity being used to calculate the isopycnal and thickness diffusion. Experiments are carried out with values of the diffusivity of 500, 1000, and 2000 m² s⁻¹. The total OHU is insensitive to these changes. The insensitivity is mainly due to the changes in the vertical heat flux by GMR mixing being compensated by changes in the other vertical heat flux components.

In the Atlantic when the diffusivity is reduced from 1000 to 500 m² s⁻¹, the surface warming can penetrate deeper. Therefore, the warming decreases by about 0.15°C above 2000 m but increases by about 0.15°C below 2500 m. Similarly, when the diffusivity is increased from 1000 to 2000 m² s⁻¹, the surface warming becomes shallower; the warming increases by about 0.2°C above 1000 m but decreases by about 0.2°C below 1000 m. These changes in the vertical distribution of the OHU also contribute to the insensitivity of the total OHU to changes in the GMR mixing. The analysis of heat flux convergence indicates that the difference of OHU seems to be associated with the MOTC circulation.

1. Introduction

The ocean regulates global climate change because of its large heat capacity. In a global warming scenario, the rate of ocean heat uptake (OHU) is a critical factor affecting the global climate change. Observations indicate a warming in the World Ocean in the past decades (Levitus et al. 2000). The warming appears to be associated with the increase of greenhouse gas concentrations according to the simulations of Levitus et al.

(2001) and Barnett et al. (2001). However, the OHU in simulations may depend strongly on how models are set up and how subgrid-scale mixing is parameterized. For example, the vertical diffusivity may have a wide range between 0.1 and 1×10^{-4} m² s⁻¹ (Zhang et al. 2001; Ledwell et al. 2000; Jenkins 1991; Nakamura and Cao 2000). The isopycnal diffusivity may range from 500 to 2000 m² s⁻¹ (Ku and Luo 1994; Hirst and Cai 1994; Jenkins 1991; Ledwell et al. 1998; Thiele 1986). Therefore, different magnitudes of simulated OHU may directly result in large differences in the projection of the future climate (Houghton et al. 2001). As indicated in the study of Huang et al. (2003a), the ocean's equilibrium heat content appears to be sensitive to the isopycnal

Corresponding author address: Dr. Boyin Huang, The Center for Research on the Changing Earth System, 10211 Wincopin Circle, Suite 240, Columbia, MD 21044.
E-mail: bhuang@wind.mit.edu

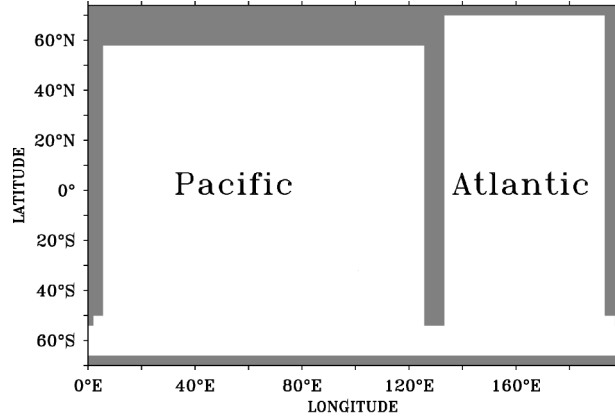


FIG. 1. Idealized topography of oceans.

and diapycnal diffusivities of temperature based on simulations with an adjoint ocean general circulation model (OGCM). The further study of Huang et al. (2003b) indicated that the OHU is largely associated with the reduction of upward heat flux due to eddy mixing. This raises the question of whether OHU is sensitive to the strength of the eddy mixing.

Using an OGCM coupled with a statistical–dynamic atmospheric model, we look at how OHU in a transient climate change depends on the strength of the eddy mixing. The coupled model is briefly described in section 2, followed by the transient response of climate in section 3. The mechanisms of OHU are diagnosed in section 4. The uncertainty of OHU due to different eddy diffusivities is analyzed in section 5. Section 6 is the summary.

2. Model

We use the Massachusetts Institute of Technology (MIT) OGCM (Marshall et al. 1997) coupled with a two-dimensional (meridional and height) statistical dynamical atmospheric model (Sokolov and Stone 1998; Kamenkovich et al. 2002, hereafter KSS). The ocean basin is set with an idealized Pacific, Atlantic, and Southern Ocean with flat bottom topography except at the Drake Passage where a sill of 1600 m is added (Fig. 1). The horizontal resolution is $4^\circ \times 4^\circ$ except near the eastern and western boundaries where a finer resolution of 1° in longitude is used so that the boundary currents can be simulated more realistically. The vertical resolution is 15 levels with the thickness ranging from 50 m near the surface to 550 m at the bottom of 4500 m. The time step of the OGCM is 30 min for momentum equations and 8 h for tracer equations. The sea ice is not included in our OGCM, but the ocean temperature is limited above -2°C .

The resolution of the atmospheric model is 7.8° latitude from 90°S to 90°N , and nine levels in the vertical from surface to 10 hPa. The time step is 20 min. The atmosphere and ocean are coupled in a time interval of 8 h,

with each model being forced by climatological boundary conditions plus anomalies generated by the other model. The ocean forces the atmosphere through the imposition of anomalies in zonal averaged sea surface temperature (SST), and the atmospheric model calculates the anomalies in the zonal averages of surface heat and freshwater fluxes, and their partial derivatives with respect to the SST. The calculated anomalous fluxes are redistributed zonally before forcing the ocean model:

$$F_o = F_a + \frac{\partial F_a}{\partial \overline{\text{SST}}} (\text{SST} - \overline{\text{SST}}), \quad (1)$$

where F_o and F_a are the anomalous fluxes into the ocean and from the atmosphere, respectively. $\overline{\text{SST}}$ is zonally averaged SST. The sea ice is calculated using a two-layer thermodynamic sea ice model. The anomaly of zonal wind stress calculated by the atmospheric model directly forces the ocean without zonal redistribution (see KSS for more detail).

Small-scale vertical diffusion of temperature and salinity are parameterized with a constant diffusion coefficient of $0.5 \times 10^{-4} \text{ m}^2 \text{ s}^{-1}$, and is treated implicitly. The convection adjustment is parameterized by an instantaneous (within one time step) mixing of the temperature and salinity between two adjacent unstable layers (Cox and Bryan 1984). Mesoscale eddies are parameterized in the MIT OGCM by the Gent–McWilliams (1990) thickness diffusion or bolus advection of tracers, in combination with the Redi (1982) diffusion along isopycnal surfaces. The thickness and isopycnal diffusivities are set equal, and have a uniform value of $1000 \text{ m}^2 \text{ s}^{-1}$ in the standard version of the model.

The Redi isopycnal diffusion is formulated as

$$\frac{\partial \tau}{\partial t} \sim \nabla \cdot K_\rho \mathbf{M}_{\text{Redi}} \nabla \tau, \quad (2)$$

where K_ρ is the diffusivity along isopycnal surface,

$$\mathbf{M}_{\text{Redi}} = \begin{pmatrix} 1 & 0 & S_x \\ 0 & 1 & S_y \\ S_x & S_y & |S|^2 \end{pmatrix}, \quad (3)$$

$$S_x = - \left(\frac{\partial z}{\partial x} \right)_\rho, \quad (4)$$

$$S_y = - \left(\frac{\partial z}{\partial y} \right)_\rho, \quad (5)$$

$$|S|^2 = S_x^2 + S_y^2, \quad (6)$$

and τ is a tracer. The Gent–McWilliams thickness diffusion (bolus advection) is formulated as

$$\frac{\partial \tau}{\partial t} \sim -\nabla \cdot \mathbf{v}^* \tau = \nabla \cdot K_{\text{GM}} \mathbf{M}_{\text{GM}} \nabla \tau, \quad (7)$$

where K_{GM} is the coefficient of thickness diffusivity, and

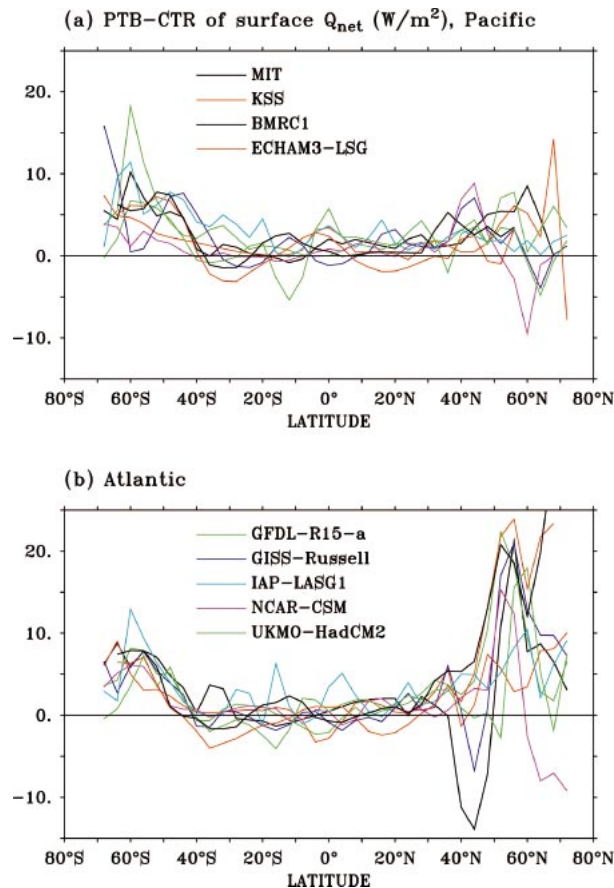


FIG. 2. Anomaly of net surface heat flux (W m^{-2} , positive downward) between PTB and CTR runs in the (a) Pacific and (b) Atlantic. The anomaly is averaged zonally and from year 61 to 80, except for MIT and KSS, which is an annual average of year 70.

$$\mathbf{M}_{\text{GM}} = \begin{pmatrix} 0 & 0 & -S_x \\ 0 & 0 & -S_y \\ S_x & S_y & 0 \end{pmatrix}. \quad (8)$$

Assume $K_\rho = K_{\text{GM}} \equiv K_I$. Now the Redi diffusion and the Gent–McWilliams thickness diffusion can be combined simply as

$$K_\rho \mathbf{M}_{\text{Redi}} + K_{\text{GM}} \mathbf{M}_{\text{GM}} = K_I \begin{pmatrix} 1 & 0 & 0 \\ 0 & 1 & 0 \\ 2S_x & 2S_y & |S|^2 \end{pmatrix}, \quad (9)$$

and are referred to as GMR mixing hereafter.

The coupled model is spun up for 2000 yr with the initial condition for the ocean taken from an ocean-alone integration of 5000-yr duration. The simulation is then separated into a control (CTR) run and a perturbation (PTB) run. The CO_2 concentration is set to 332 ppm in CTR, but increases at $1\% \text{ yr}^{-1}$ for 75 yr and is kept constant for 400 yr in PTB, which can be thought of as a global warming scenario.

The evolution of our coupled ocean–atmosphere system is comparable with other atmosphere–ocean GCMs

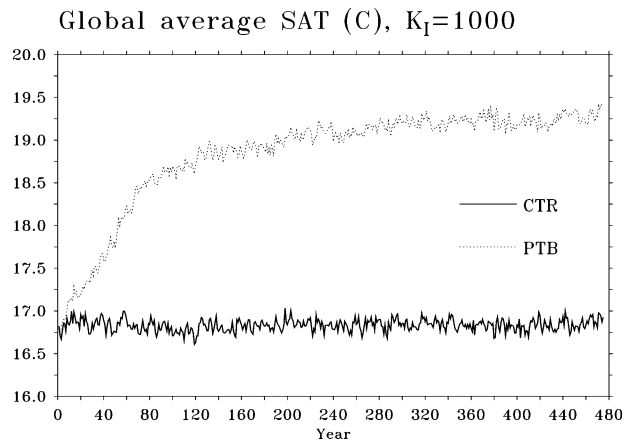


FIG. 3. Temporal evolution of global average SAT ($^{\circ}\text{C}$) in PTB and CTR runs.

(AOGCMs). For example, as shown in Fig. 2, our simulation (indicated as MIT) shows that the zonally and annually averaged anomaly of surface heat flux at the time of CO_2 doubling (year 70) is about 7 W m^{-2} in the Southern Ocean south of 50°S , and 20 W m^{-2} in the North Atlantic north of 50°N . The heat flux anomaly in our simulation is consistent with the simulation of KSS. KSS used the Geophysical Fluid Dynamics Laboratory (GFDL) OGCM with the same ocean configuration as ours, and coupled it with the same statistical–dynamical atmospheric model. Our simulation is also consistent with the simulations of fully coupled AOGCMs from the Climate Model Intercomparison Project-2 (CMIP-2). That project used the same scenario as ours, with CO_2 increasing $1\% \text{ yr}^{-1}$. The changes in a number of the CMIP models’ surface heat flux averaged zonally are shown in Fig. 2. The models included are the Bureau of Meteorology Research Centre model (BMRC1; Power et al. 1993), European Centre Hamburg Large Scale Geotrophic OGCM (ECHAM3-LSG; Voss et al. 1998), the Geophysical Fluid Dynamics Laboratory model (GFDL-R15-a; Manabe et al. 1991), the Goddard Institute for Space Studies model (GISS-Russell; Russell et al. 1995), the Institute of Atmospheric Physics Laboratory for Atmospheric Sciences and Geophysical Fluid Dynamics model (IAP-LASG1; Zhang et al. 2000), the National Center for Atmospheric Research Climate System Model (NCAR-CSM; Boville and Gent 1998), and the Met Office-Hadley Centre second-generation coupled GCM (UKMO-HadCM2; Johns et al. 1997).

3. Transient response

As indicated in Fig. 2, our model can simulate the heat forcing from the atmosphere such as other AOGCMs, but how about the transient response of the ocean to the atmospheric warming due to the increases of CO_2 concentration? Figure 3 shows the evolution of

TABLE 1. Anomalies of global averaged SAT ($^{\circ}\text{C}$) and Atlantic MOTC (Sv) between PTB and CTR runs at the time of CO_2 concentration doubling (year 70).

Models	ΔSAT ($^{\circ}\text{C}$)	ΔMOTC (Sv)
MIT	1.7	4.5
KSS	1.6	4.5
BMRC1	1.4	N/A
ECHAM3-LSG	1.3	5
GFDL_R15_a	2.2	5
GISS-Russell	1.4	3
IAP-LSAG1	1.7	2
NCAR-CSM	1.4	1
UKMO-HadCM2	1.7	6.5

global average surface air temperature (SAT) in the global warming scenario. At the time of CO_2 concentration doubling (year 70), the SAT anomaly is about 1.7°C . The SAT anomaly increases further and reaches to about 2.5°C approximately at year 475. The magnitude of SAT anomaly is consistent with the simulation of KSS and other fully coupled models from the CMIP-2 (Table 1). The SAT anomaly in these models ranges from 1.3° to 2.3°C at the time of CO_2 doubling according to simulations from BMRC1 (Power et al. 1993; Colman et al. 1995), ECHAM3-LSG (Cubasch et al. 1992), GFDL_R15_a (Manabe et al. 1991), GISS-Russell (Russell and Rind 1999), UKMO-HadCM2 (Murphy and Mitchell 1995), IAP-LSAG1 (Guo et al. 2001), and NCAR-CSM (Meehl et al. 2000).

The strength of the maximum overturning circulation (MOTC) in the North Atlantic is reduced (Fig. 4a) as the ocean warms. The MOTC decreases from about 29 Sv ($1 \text{ Sv} \equiv 10^6 \text{ m}^3 \text{ s}^{-1}$) to 24 Sv at the time of CO_2 concentration doubling, and decreases further to about 23 Sv at year 120. The MOTC recovers gradually to about 26 Sv at year 475. The reduction of MOTC is about 4.5 Sv at the time of CO_2 concentration doubling, which is also consistent with the simulations of KSS and CMIP-2 models (Table 1).

The strength and speed of the recovery of the MOTC after CO_2 stabilization varies from model to model. As indicated in the studies of Stouffer and Manabe (1999) and Manabe and Stouffer (1994), the MOTC recovers completely at the end of year 500. The study of Wiebe and Weaver (1999), who used the GFDL OGCM coupled with an energy–moisture balance model, indicates that the MOTC decreases from 24.5 to 22.5 Sv and then recovers rapidly and overshoots to about 29 Sv.

Interestingly, our simulation shows that the MOTC is located at about 45°N and 1350 m (Table 2) in the North Atlantic in CTR (Fig. 5a), which is consistent with the simulation of KSS. The center of MOTC drifts upward to 1050 m in PTB. As a result, the OTC cell becomes shallower and the transport of Antarctic Bottom Water (AABW) increases by about 2 Sv, which are consistent with the simulation of Stouffer and Manabe (1999). The shallower MOTC and large AABW are also indicated in the OTC anomaly between PTB and CTR

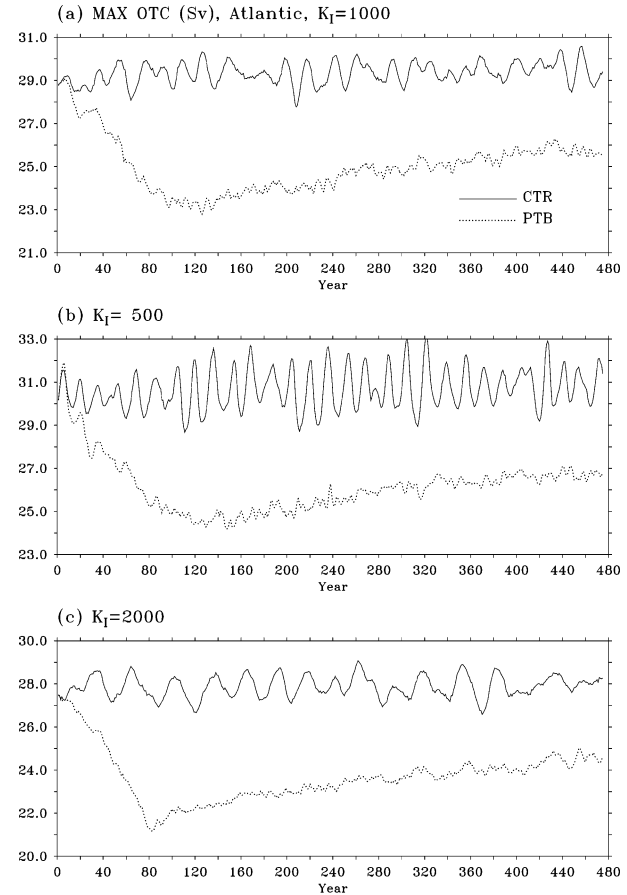


FIG. 4. Temporal evolution of MOTC (Sv) in the Atlantic in PTB and CTR runs: (a) $K_I = 1000$, (b) $K_I = 500$, and (c) $K_I = 2000 \text{ m}^2 \text{ s}^{-1}$.

(Fig. 5b). The center of the OTC anomaly is located at about 2700 m and 60°N (Table 2). The magnitude of the OTC anomaly is about 14 Sv, which is much larger than the MOTC reduction of 4.5 Sv (refer to Fig. 4a). The large OTC anomaly in the North Atlantic appears to be associated with the stronger heat flux from the atmosphere as shown in Fig. 2b. In contrast, the OTC anomaly in the Pacific is only about 2 Sv, and its location does not coincide with the minimum OTC either (not shown). The patterns of OTC and its anomaly in the Atlantic dominate the global pattern.

Furthermore, we note that the magnitude and location of the OTC anomaly do not have any recovery after year 80 (Figs. 6 and 5b). The indication is that the

TABLE 2. Depth (m) of MOTC in CTR and PTB, of OTC anomaly between PTB and CTR, and of penetration of warming (POW) in the Atlantic by year 475.

K_I ($\text{m}^2 \text{ s}^{-1}$)	CTR	PTB	PTB – CTR	POW
1000	1350	1050	2700	3360
500	1350	1060	3200	3540
2000	1240	950	2250	3130

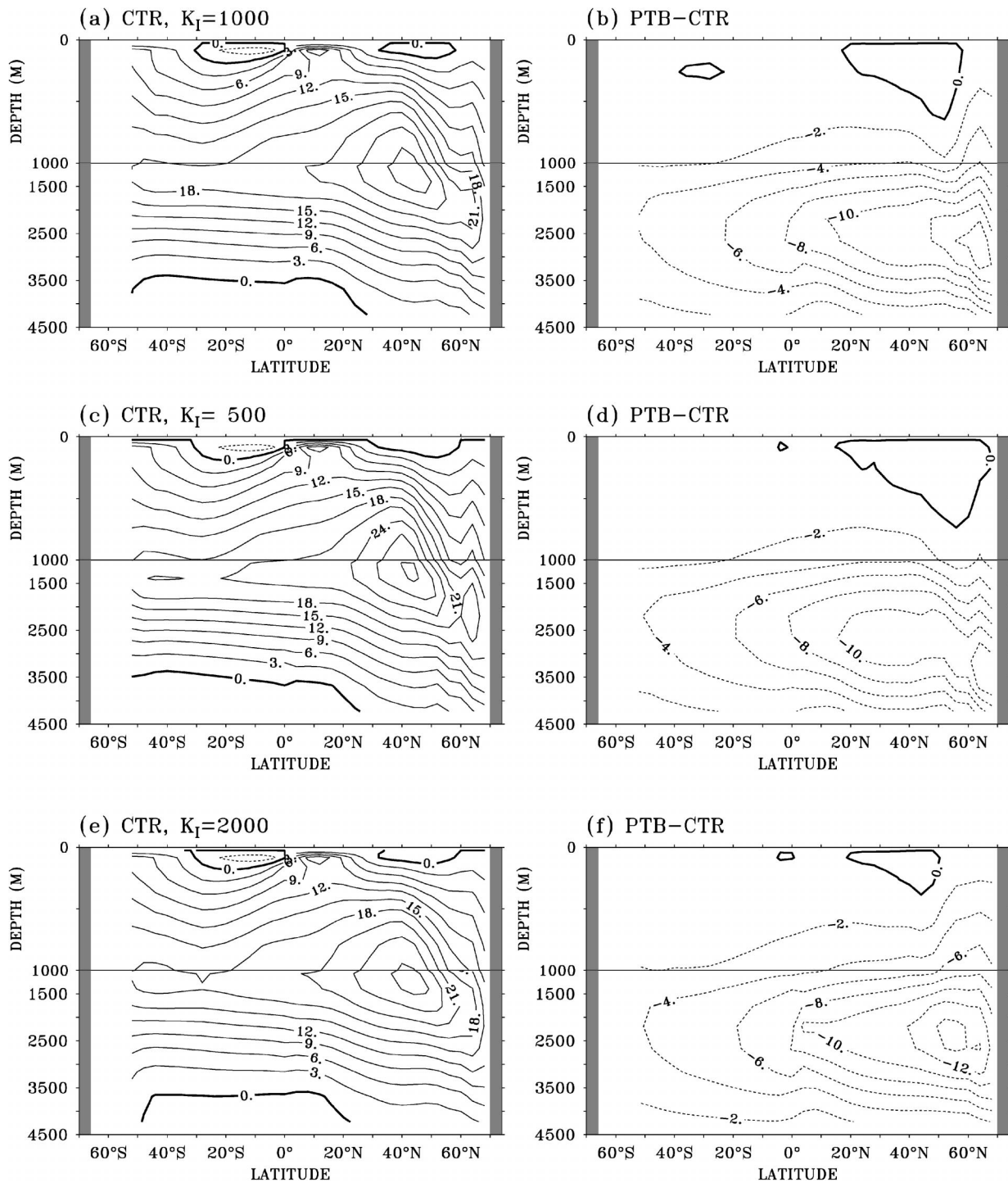


FIG. 5. OTC in (a) global, (c) Pacific, and (e) Atlantic in CTR run, and (b), (d), (f) its anomaly between PTB and CTR runs, respectively. It is averaged from year 66 to 75. The contour intervals (CIs) are 3 Sv in (a), (c), and (e), but 2 Sv in (b), (d), and (f). Solid (dotted) contours indicate sinking in the north (south).

MOTC in the North Atlantic may at least partly recover when CO_2 concentration is kept constant after doubling, but its effect on the deep circulation below 3000 m does not disappear.

In the meantime, the ocean temperature increases gradually as the atmospheric heat flux into the ocean increases. By year 70, the ocean temperature increases by about 1°C near the surface, and 0.1°C at 1000 m in

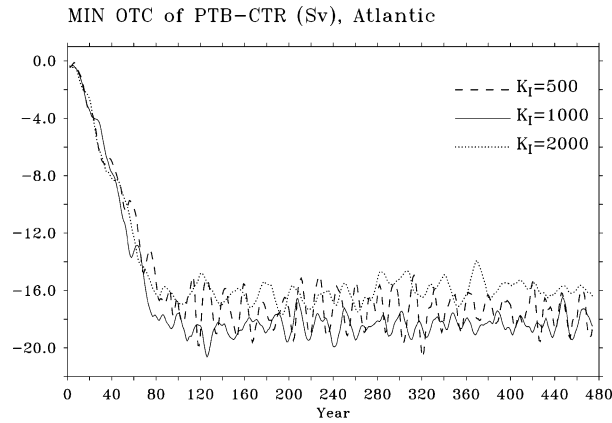


FIG. 6. Temporal evolution of the minimum of OTC anomaly (Sv) between PTB and CTR runs, when GMR diffusivity is set to 500, 1000, and 2000 $\text{m}^2 \text{s}^{-1}$.

the Pacific and 0.3°C in the Atlantic (Fig. 7). The temperature anomaly between PTB and CTR penetrates deeper in the Atlantic than in the Pacific, which is associated with strong convection and GMR mixing in the North Atlantic (Huang et al. 2003a). The surface warming can penetrate down to 3360 m as shown in Fig. 8a and Table 2. On the other hand, there is a cooling of 0.5°C in the North Atlantic at about 60°N and 4000-m depth. The detailed mechanisms of OHU will be discussed in the next section. Overall, the temperature anomaly in our simulation appears to be comparable with the simulation of the GFDL model (Manabe et al. 1991).

4. Mechanisms of ocean heat uptake

As indicated in an earlier study of Huang et al. (2003b) using the adjoint version of the MIT OGCM, the OHU appears to be due primarily to the reduction of upward heat flux by GMR mixing. To diagnose the mechanisms of OHU in transient climate change, we write the zonally averaged ocean temperature equation as

$$\rho c_p \frac{\partial T}{\partial t} = -\partial_y(F_{VT}) - \partial_z(F_{WT}) - \partial_z(F_{GMR}) - \partial_z(F_{CV}) - \partial_z(F_{DD}), \quad (10)$$

where

$$F_{VT} = \rho c_p VT, \quad (11)$$

$$F_{WT} = \rho c_p WT, \quad (12)$$

$$F_{DD} = -\rho c_p \kappa \frac{\partial T}{\partial z} - Q_s, \quad (13)$$

are heat fluxes of meridional advection, vertical advection, and vertical diffusion, respectively. Here Q_s is the surface heat flux from the atmosphere, and F_{GMR} and F_{CV} are vertical heat fluxes due to GMR mixing and convection, respectively. Other terms such as meridional

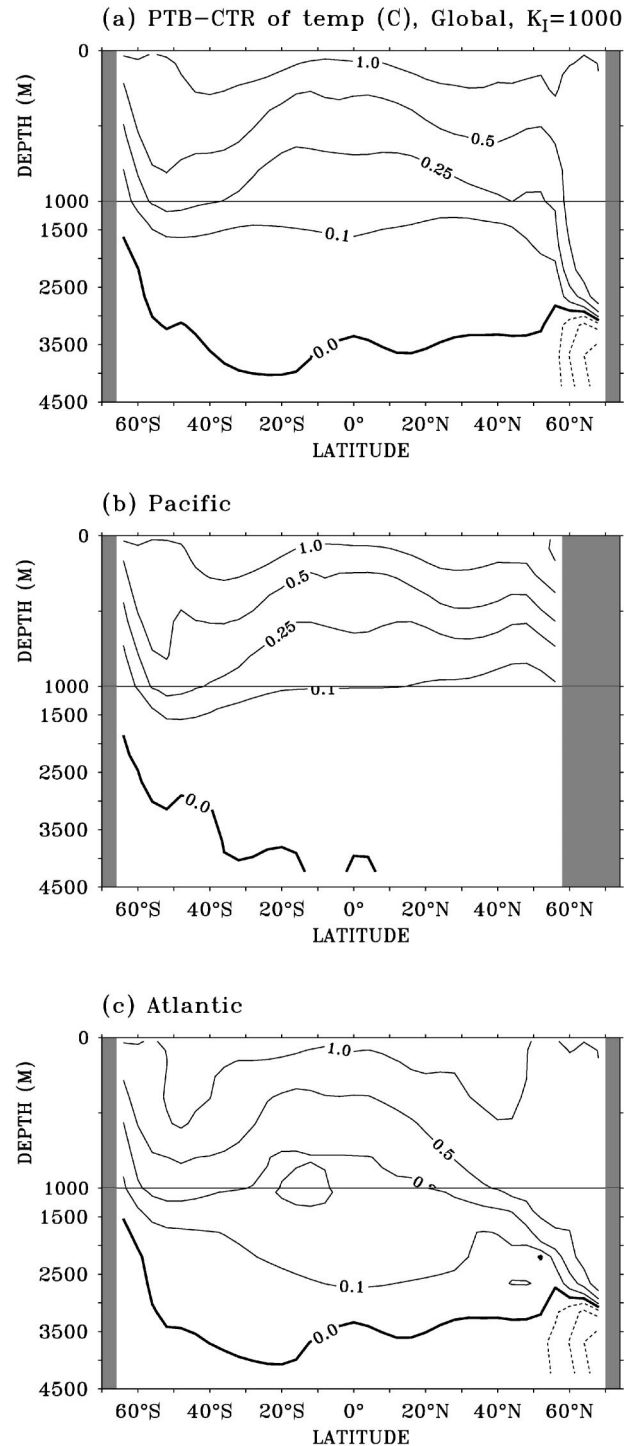


FIG. 7. Temperature anomaly between PTB and CTR in (a) global, (b) Pacific, and (c) Atlantic. It is averaged zonally and from year 66 to 75. The CIs are $\pm 0.1^\circ$, $\pm 0.25^\circ$, $\pm 0.5^\circ$, and $\pm 1.0^\circ\text{C}$. Negative contours are dotted.

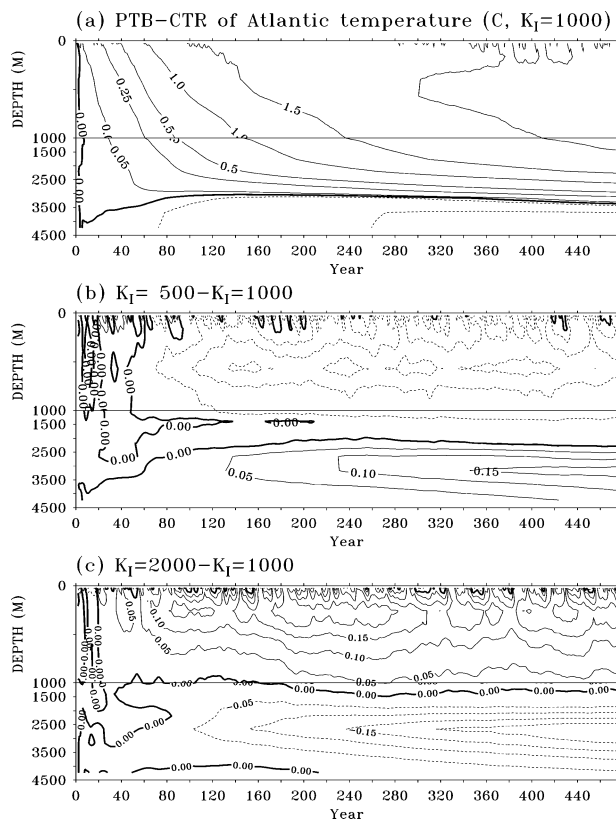


FIG. 8. (a) Temporal evolution of temperature anomaly between PTB and CTR runs averaged in the Atlantic. (b) The difference of temperature anomalies between GMR diffusivity 500 and $1000 \text{ m}^2 \text{ s}^{-1}$, and (c) between GMR diffusivity 2000 and $1000 \text{ m}^2 \text{ s}^{-1}$. The CIs are $\pm 0.05^\circ$, $\pm 0.25^\circ$, $\pm 0.5^\circ$, $\pm 1^\circ$, $\pm 1.5^\circ$, and $\pm 2^\circ \text{C}$ in (a), but $\pm 0.05^\circ$, $\pm 0.1^\circ$, $\pm 0.15^\circ$, and $\pm 0.2^\circ \text{C}$ in (b) and (c).

heat flux convergence due to GMR mixing are negligible. The sum of the right-hand side of (10) contributes to the temperature change, which is zero in CTR. By diagnosing the anomalies of these heat flux convergences between PTB and CTR we will have a better understanding about the mechanisms controlling the OHU. However, we will only present the diagnosis in the Atlantic where the warming and OTC anomaly are large.

Figure 9 shows the anomalies of heat flux convergence between PTB and CTR averaged zonally and from year 1 to 75. By comparing Figs. 9a and 7c, it is very clear that the pattern and relative magnitude of temperature anomaly between PTB and CTR during year 66 and 75 are well consistent with the average anomaly of net heat flux convergence between year 1 and 75. The large temperature increase in the upper ocean is associated with a strong anomaly of net heat flux convergence. The decrease of deep ocean temperature below 3000 m in the North Atlantic is in accord with the anomaly of heat flux divergence. The only exception is at about 200 m in the North Atlantic near 30°N and 55°S , which may result from the inconsistency between

our explicit diagnosis of the vertical diffusion and its implicit prognosis in the model integration.

By comparing the anomaly distributions of net heat flux convergence and its five major components, we see that no one factor dominates the ocean temperature anomaly. Rather, we can see a clear cancellation between anomalies of heat flux convergences in meridional and vertical advection (magnitudes of $5\text{--}20 \times 10^{-10} \text{ K s}^{-1}$; Figs. 9b and 9c) almost throughout the entire Atlantic. The cancellation can also be seen between heat flux convergences due to GMR mixing, convection, and vertical diffusion (magnitudes of $5\text{--}20 \times 10^{-10} \text{ K s}^{-1}$; Figs. 9d–f) in the North Atlantic and the Southern Ocean. The anomaly of net heat flux convergence appears to be a small residual of convergence anomalies of different heat flux components.

To clarify how the oceanic temperature anomaly is associated with different oceanic dynamic processes, we combine the anomaly of heat flux convergence due to large-scale advection (Fig. 10a) and the one due to sub-grid-scale mixing and convection (Fig. 10b). From Fig. 10, we can conclude that the warming between PTB and CTR in the Atlantic between 200 and 3500 m and between 50°S and 40°N is associated with the increase of heat flux convergence ($1\text{--}2 \times 10^{-10} \text{ K s}^{-1}$) due to large-scale advection. In contrast, the heat flux anomaly due to large-scale advection is divergent north of 40°N (Fig. 10a), which is obviously associated with the weakening of OTC in the Atlantic as indicated in Figs. 4a and 5b. Indeed, the warming in the North Atlantic north of 40°N and the Southern Ocean above 1000 m is associated with the increase of eddy heat flux convergence ($2\text{--}5 \times 10^{-10} \text{ K s}^{-1}$) due to convection (cf. Figs. 10b and 9f) and GMR mixing (cf. Figs. 10b and 9d). The increase of vertical diffusive heat flux convergence is mainly located in the Tropics due to the strong vertical temperature gradient. These results are largely consistent with the simulation study of Gregory (2000).

In the global average, the vertical penetration of surface heat into the deep ocean is largely associated with the reduction of convection ($0.1\text{--}0.6 \text{ W m}^{-2}$) above 1000 m (Fig. 11a), and with the reduction of upward GMR mixing (0.1 W m^{-2}) between 1000 and 2500 m. The cooling in the deep Atlantic below 3000 m is also understandable. The OTC is reduced as the surface ocean becomes warmer especially in the higher latitudes. The reduction of OTC results in less downward heat flux to the deep ocean, although it does transport more heat in the upper ocean due to the increase of temperature. Therefore, the lower ocean is cooled rather than warmed.

5. Uncertainty

To estimate the uncertainty of OHU in the global warming scenario due to GMR mixing (K_I), we ran additional model simulations by setting K_I to 500 and $2000 \text{ m}^2 \text{ s}^{-1}$, respectively. These simulations are com-

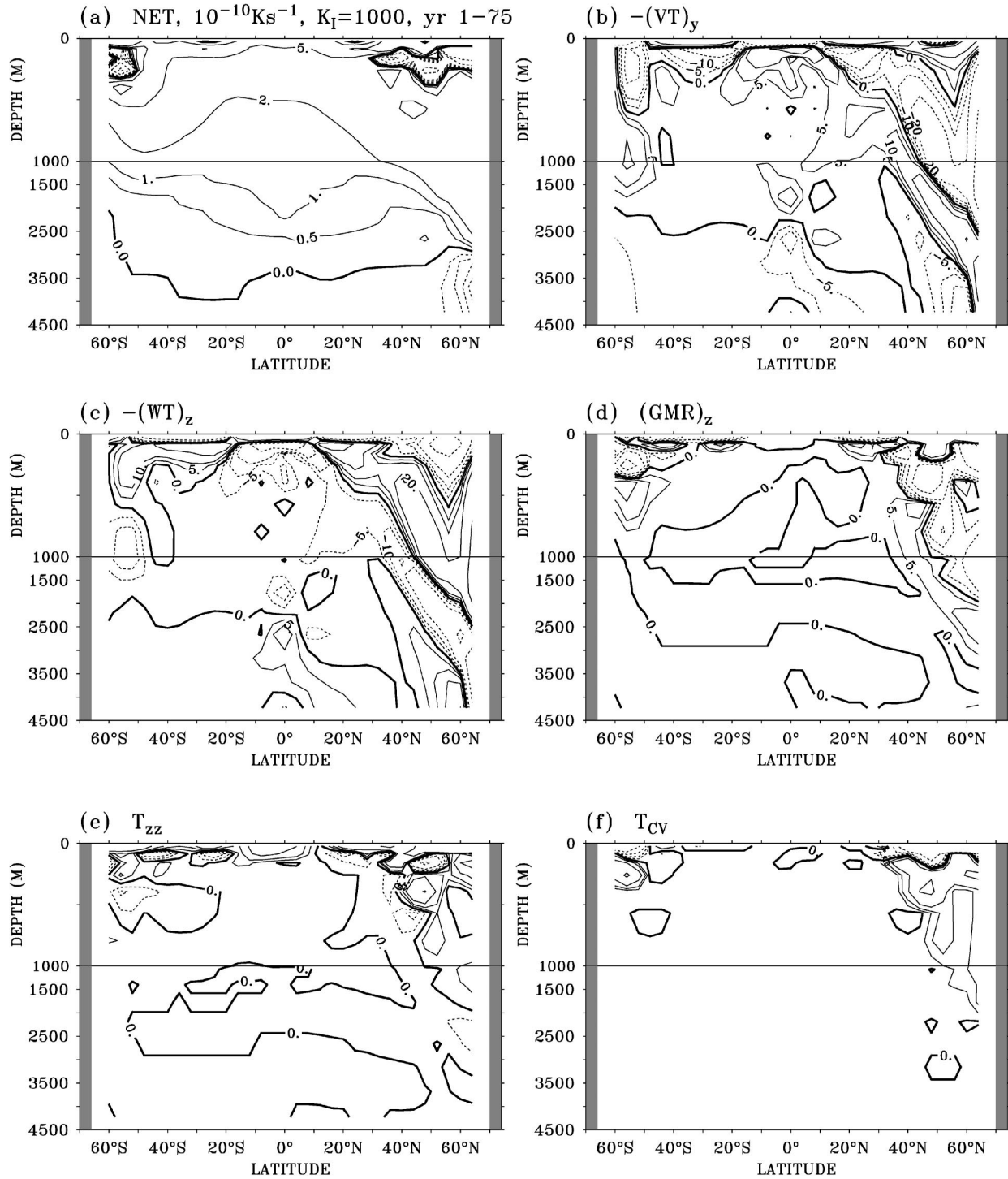


FIG. 9. Anomaly of heat flux convergence between PTB and CTR runs: (a) net, (b) meridional advection, (c) vertical advection, (d) GMR mixing, (e) vertical diffusion, and (f) convection. It is averaged zonally in the Atlantic and from year 1 to 75. The CIs are ± 0.5 , ± 1 , ± 2 , and $\pm 5 \times 10^{-10} \text{ K s}^{-1}$ in (a), but ± 5 , ± 10 , and $\pm 20 \times 10^{-10} \text{ K s}^{-1}$ in (b)–(f). Positive (negative) indicates convergence (divergence).

pared with the standard run in which K_I is set to $1000 \text{ m}^2 \text{ s}^{-1}$. The range of K_I from 500 to $2000 \text{ m}^2 \text{ s}^{-1}$ may be reasonable based on observations at different oceanic locations and of eddies at different spatial scales (Ku

and Luo 1994; Hirst and Cai 1994; Jenkins 1991; Ledwell et al. 1998; Thiele 1986).

We want to remind readers that the OHU is defined as the difference of ocean temperature or heat capacity

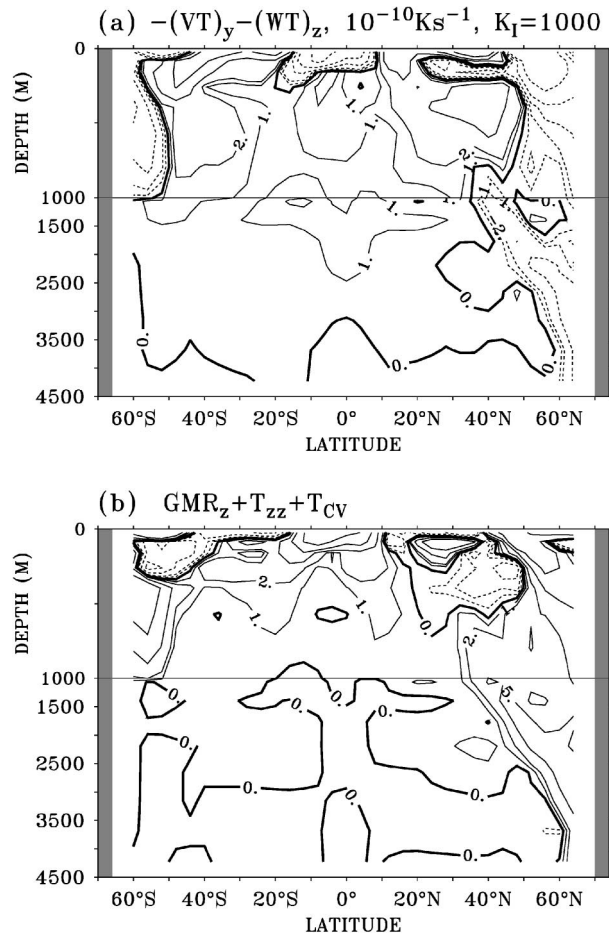


FIG. 10. Combined anomaly of heat flux convergence between PTB and CTR runs. (a) Meridional and vertical advection, and (b) GMR mixing, vertical diffusion, and convection. It is averaged zonally in the Atlantic and from year 1 to 75. The CIs are ± 1 , ± 2 , ± 5 , and $\pm 10 \times 10^{-10} \text{K s}^{-1}$.

between the PTB and CTR runs when CO_2 concentration is changed. That is to say, the difference among CTR runs using three different K_I is excluded. Our simulations of CTR runs indicate (not shown) that the ocean temperature increases by about 1.2°C between 100 and 1500 m, and about 0.5°C below 2000 m when K_I decreases from 1000 to $500 \text{ m}^2 \text{ s}^{-1}$. Likewise, the ocean temperature decreases by about 1.2°C between 100 and 1500 m, and about 0.3°C below 2000 m when K_I increases from 1000 to $2000 \text{ m}^2 \text{ s}^{-1}$. Corresponding with the ocean temperature change, the MOTC of CTR runs in the Atlantic increases by about 4 Sv when K_I decreases from 1000 to $500 \text{ m}^2 \text{ s}^{-1}$, but decreases by about 2 Sv when K_I increases from 1000 to $2000 \text{ m}^2 \text{ s}^{-1}$ (Figs. 5a,c, and 5e). The reason is that when K_I decreases (increases), the convection have to be stronger (weaker) to balance the vertical heat flux due to vertical advection and diffusion (Huang et al. 2003a). The stronger (weaker) convection enhances (weakens) the MOTC, which eventually increases (decreases) the ocean temperature.

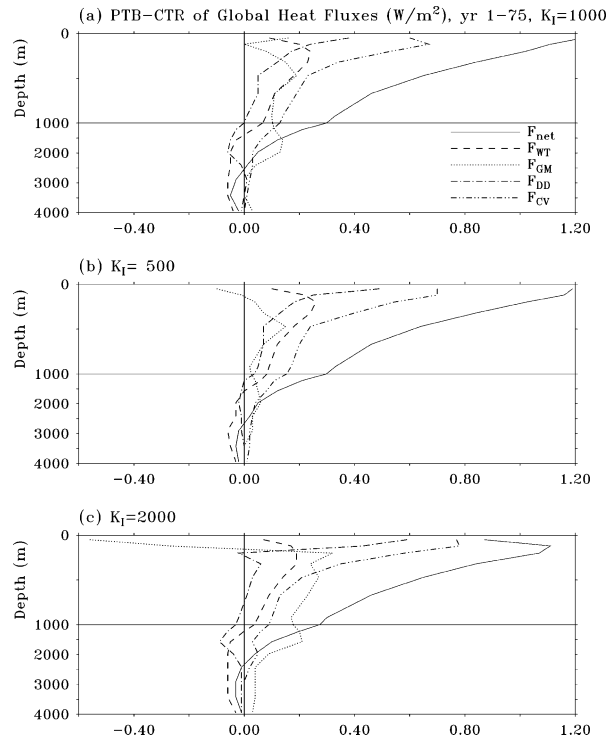


FIG. 11. Anomaly of global vertical heat flux (W m^{-2} , positive downward) between PTB and CTR runs. It is averaged globally and from year 1 to 75. (a) $K_I = 1000$, (b) $K_I = 500$, and (c) $K_I = 2000 \text{ m}^2 \text{ s}^{-1}$.

Similar to the reasons for analyzing OHU mechanisms in the Atlantic, we will only discuss the uncertainty of ocean heat uptake due to K_I in the Atlantic. The changes in the Pacific are similar but with smaller magnitude and slightly different vertical distribution.

a. Temporal evolution

First, we find that the evolution of MOTC in the North Atlantic for K_I of 500 and $2000 \text{ m}^2 \text{ s}^{-1}$ follows almost the same trajectory as for K_I of $1000 \text{ m}^2 \text{ s}^{-1}$ (Figs. 4a-c). In all three cases, the OTC anomaly below 3000 m persists after year 100 (Fig. 6). The difference of minimum OTC anomaly between PTB and CTR when K_I is set to $2000 \text{ m}^2 \text{ s}^{-1}$ is about 2 Sv larger than that when K_I is set to $1000 \text{ m}^2 \text{ s}^{-1}$. However, we should note that the depth of these minimum OTC anomalies is different as indicated in Figs. 5d,f, and Table 2.

The total OHU is very insensitive to the changes in the eddy mixing, as shown in Table 3. This is primarily

TABLE 3. Total OHU ($\times 10^{24} \text{ J}$) in different basins by year 475.

K_I ($\text{m}^2 \text{ s}^{-1}$)	Global	Pacific	Atlantic
1000	3.91	2.24	1.67
500	3.90	2.20	1.70
2000	3.77	2.19	1.58

because when the GMR mixing and the associated vertical heat flux increase, there are compensating decreases in the other vertical heat fluxes, as shown in Figs. 11a–c. For example, at 500 m, when K_I is increased from 500 to $2000 \text{ m}^2 \text{ s}^{-1}$, the associated flux anomaly doubles, but there is no change in the net flux anomaly because of decreases in the other fluxes.

The insensitivity of OHU to the changes in the eddy mixing is also due in part to the changes in the vertical distribution of OHU in the Atlantic. As briefly discussed in section 3, the ocean temperature in the Atlantic increases gradually near the surface, and propagates downward to about 3360 m (Table 2) as indicated in Fig. 8a, when K_I is $1000 \text{ m}^2 \text{ s}^{-1}$. In contrast, the ocean temperature decreases slightly below 3500 m (Fig. 8a). When a smaller K_I of $500 \text{ m}^2 \text{ s}^{-1}$ is used (Fig. 8b), the difference in the warming anomalies becomes notable after year 80. The warming anomaly penetrates down to about 3540 m (Table 2), which is about 180 m deeper than that when K_I is $1000 \text{ m}^2 \text{ s}^{-1}$. Therefore, the warming above 2000 m is reduced. The maximum reduction is about 0.15°C at near 500 m. On the other hand, the warming between 2200 and 3500 m is enhanced and the cooling below 3000 m is reduced, which results in a maximum difference of about 0.15°C at about 3500 m. The differences in temperature anomalies in the Atlantic between K_I of 500 and $1000 \text{ m}^2 \text{ s}^{-1}$ largely cancel between the upper and lower ocean, thus helping to keep the global OHU virtually the same at $3.9 \times 10^{24} \text{ J}$ by year 475 (Table 3).

When a larger K_I of $2000 \text{ m}^2 \text{ s}^{-1}$ is used (Fig. 8c), the pattern of the difference of warming anomalies in the Atlantic appears to be opposite to that when a smaller K_I of $500 \text{ m}^2 \text{ s}^{-1}$ is used. The warming anomaly penetrates down to about 3130 m (Table 2), which is about 230 m shallower than that when K_I is $1000 \text{ m}^2 \text{ s}^{-1}$. The warming above 1000 m is enhanced starting from year 20. The maximum enhancement is about 0.2°C at about 250 m. The enhancement of warming anomaly exhibits a complex spatial structure. The warming anomaly is reduced between 1000 and 3000 m, and the cooling anomaly is enhanced below 3500 m after year 80. These changes result in a difference in OHU of about -0.2°C at 2700 m by year 475. Overall, the effect of different K_I on the OHU is small on the timescale shorter than 80 yr, but might have a large effect in the longer term. More importantly, the pattern of OHU between the upper and lower ocean is changed, which may further modify the stability of the ocean and have an important impact on the OTC evolution. The change of OHU distribution may also impact on the sea level rise pattern.

b. Spatial distribution

The warming in the Atlantic is relatively strong in the higher latitudes between year 66 and 75 as shown in Fig. 7c when K_I is set to $1000 \text{ m}^2 \text{ s}^{-1}$. The same

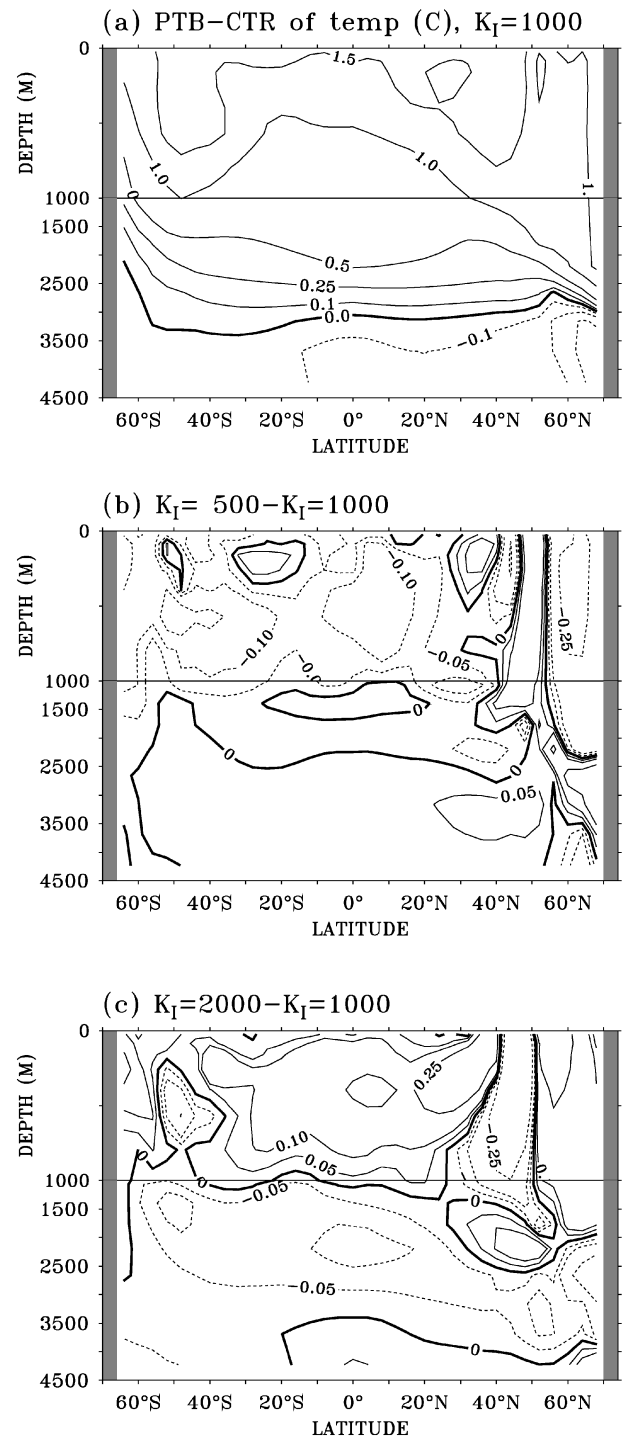


FIG. 12. (a) Temperature anomaly in the Atlantic between PTB and CTR runs averaged from year 81 to 180. (b) The difference of temperature anomaly between GMR diffusivity 500 and $1000 \text{ m}^2 \text{ s}^{-1}$, and (c) between GMR diffusivity 2000 and $1000 \text{ m}^2 \text{ s}^{-1}$. The CIs are $\pm 0.1^\circ$, $\pm 0.25^\circ$, $\pm 0.5^\circ$, $\pm 1^\circ$, and $\pm 1.5^\circ\text{C}$, in (a), but $\pm 0.05^\circ$, $\pm 0.1^\circ$, and $\pm 0.25^\circ\text{C}$ in (b) and (c).

feature is found in the simulation between year 81 and 180 (Fig. 12a), except that the strength of warming in the upper ocean and cooling in the lower ocean increases. We average over 100 yr to remove possible interannual and interdecadal fluctuation, so we may compare temperature anomalies in simulations with different K_I .

When a small K_I of $500 \text{ m}^2 \text{ s}^{-1}$ is applied, the warming is about 0.1°C weaker above 2000 m as indicated in Fig. 8b, which is distributed throughout almost the entire Atlantic (Fig. 12b). However, the warming becomes 0.1°C stronger in a narrow band near 50°N penetrating from the surface to 1500 m, and 0.05°C stronger north of 20°N below 2500 m. In contrast, when a larger K_I of $2000 \text{ m}^2 \text{ s}^{-1}$ is applied, the warming is about 0.1°C stronger above 1000 m as indicated in Fig. 8c, which is distributed throughout the Atlantic (Fig. 12c). But, the warming is weaker in two narrow regions near 45°N and 50°S . The cooling becomes stronger below 1000 m, which appears to be distributed almost throughout the Atlantic (Fig. 12c). Overall, the different warming pattern in the upper and lower ocean at different K_I is somewhat uniformly distributed except for a narrow region of the North and South Atlantic.

c. Mechanisms

The change of OHU pattern in the North Atlantic looks to be associated with a change of the circulation anomaly in the North Atlantic when different K_I is applied. Figure 13a shows the OTC anomaly in the North Atlantic between year 81 and 180 when K_I is $1000 \text{ m}^2 \text{ s}^{-1}$. The pattern of a large anomaly of deep OTC near 65°N is very similar to the average between year 66 and 75 as shown in Fig. 5b, although the magnitude of anomaly increases to 18 Sv between year 81 and 180. When a small K_I of $500 \text{ m}^2 \text{ s}^{-1}$ is applied, there is a change of circulation anomaly of about 5 Sv near 60°N and 2000 m where a larger OHU occurs (see Fig. 13b). In contrast, when a large K_I of $2000 \text{ m}^2 \text{ s}^{-1}$ is applied, there is an opposite change of local circulation anomaly of about 4 Sv near 50°N and 1000 m where a smaller OHU occurs (see Fig. 13c).

The stronger warming near 50°N (Fig. 12b) is associated with weaker downwelling (Fig. 13b). The weaker warming near 45°N (Fig. 12c) is associated with stronger downwelling (Fig. 13c). The indication is that the change of circulation anomaly may contribute to the difference of OHU in the global warming scenario when a different K_I is applied. As indicated in Fig. 14, the anomaly of meridional and vertical heat flux convergence is very consistent with that of temperature anomaly above 1000 m (Fig. 12c) when K_I is set to $2000 \text{ m}^2 \text{ s}^{-1}$. Therefore, we think that the change of OHU may be associated with these changes of circulation anomaly when K_I is set differently, although the OHU itself is mainly associated with convection and GMR mixing as discussed in section 4. But, we have to note that the

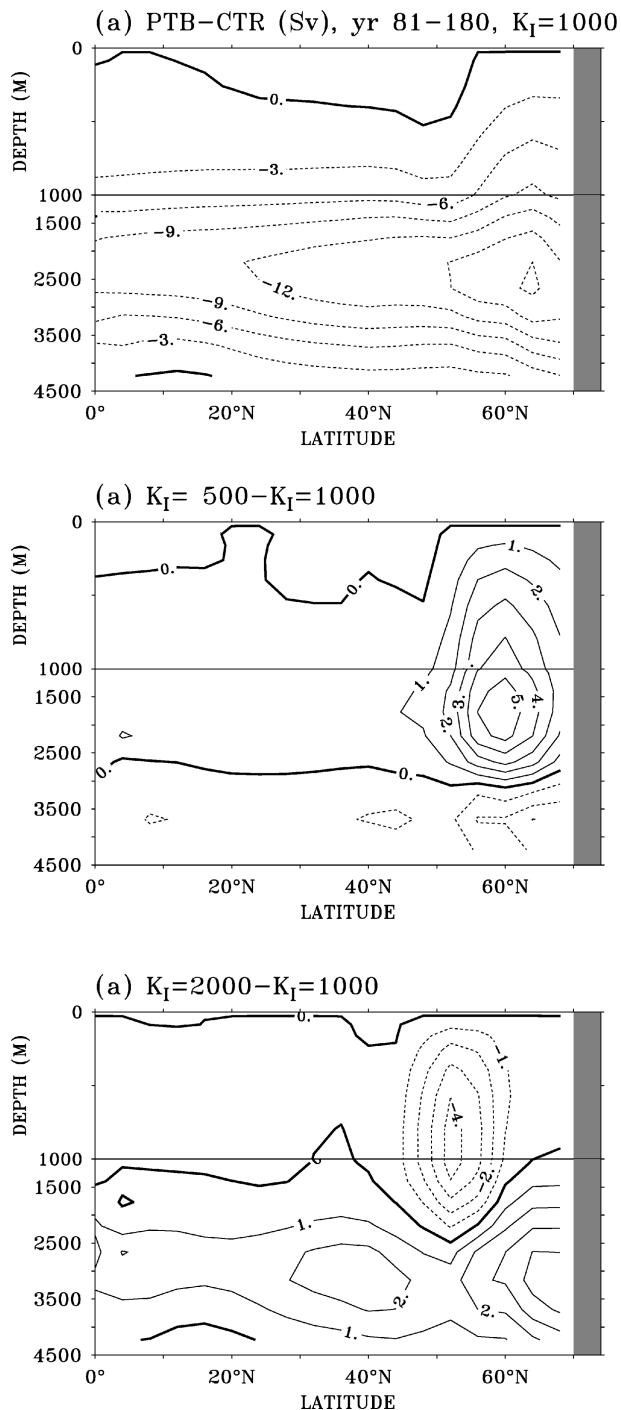


FIG. 13. (a) OTC anomaly in the Atlantic between PTB and CTR averaged from year 81 to 180. (b) The difference of OTC anomalies between GMR diffusivity 500 and $1000 \text{ m}^2 \text{ s}^{-1}$, and (c) between GMR diffusivity 2000 and $1000 \text{ m}^2 \text{ s}^{-1}$. The CIs are 3 Sv in (a), but 1 Sv in (b) and (c). Solid (dotted) contours indicate sinking in the north (south).

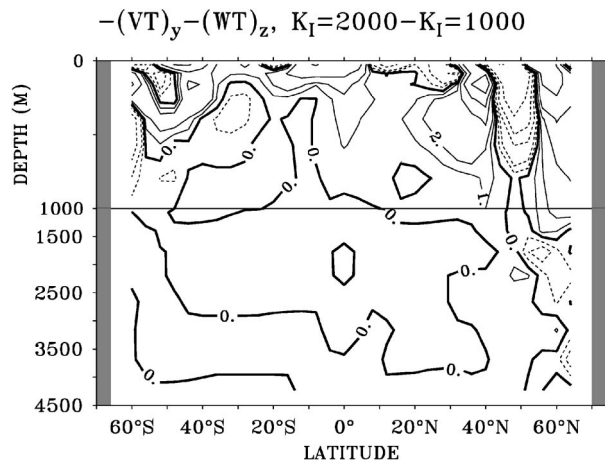


FIG. 14. Anomaly of meridional and vertical advective heat flux convergence between PTB and CTR runs, when GMR diffusivity is set to $2000 \text{ m}^2 \text{ s}^{-1}$. It is averaged from year 81 to 180. The CIs are $\pm 1, \pm 2, \pm 5, \pm 10, \text{ and } \pm 20 \times 10^{-10} \text{ K s}^{-1}$. Solid (dotted) contours indicate convergence (divergence).

pattern of different advective heat flux convergence is not clear below 1000 m.

6. Summary

The ocean heat uptake is studied using the MIT OGCM coupled with a statistical–dynamical atmospheric model when different GMR (Gent–McWilliams–Redi) diffusivities (K_I) are applied. The magnitudes of SAT increase and MOTC reduction at the time of CO_2 concentration doubling (year 70) are consistent with the simulations of coupled AOGCMs. By year 70, the SAT increases by about 1.7°C ; the depth of MOTC is about 300 m shallower; and the strength of MOTC is reduced by about 4.5 Sv when K_I is set to $1000 \text{ m}^2 \text{ s}^{-1}$. The strength of MOTC recovers gradually during next 400-yr simulation period when CO_2 concentration is kept constant. The evolution of MOTC appears to be different in the simulations of different models (Stouffer and Manabe 1999; Wiebe and Weaver 1999). But, the center of MOTC remains at the shallower depth through our simulation period of 475 yr.

The ocean temperature increases by about 1.0°C near the surface, 0.1°C at depth of 1000 m in the Pacific, and 0.3°C in the Atlantic at the time of CO_2 concentration doubling. However, the ocean temperature decreases by about 0.5°C in a small region of the North Atlantic north of 50°N below 3000 m due to increased AABW. The pattern of ocean temperature anomaly is maintained throughout our simulation period of 475 yr, although the magnitude of warming and cooling increases gradually.

The warming in the Atlantic above 3000 m between 50°S and 50°N is largely associated with the increase of advective heat flux convergence. The advective warming may be associated with stronger advection to-

ward the equator in the Tropics and stronger subduction in the subtropics. In contrast, the warming in the higher latitudes appears to be associated with convection and GMR mixing. In the global average, the OHU is mainly attributed to the reduction of convection and GMR mixing.

The total OHU is insensitive to the GMR diffusivity, mainly because changes in the GMR vertical heat flux are largely compensated by changes in the other vertical heat fluxes. The vertical distribution of the heat uptake is however changed when the GMR diffusivity is changed. When it is reduced from 1000 to $500 \text{ m}^2 \text{ s}^{-1}$, the surface warming penetrates to 3540 m instead of 3360 m in the Atlantic due to relatively stronger MOTC. Thus, the warming of the upper Atlantic above 2000 m is reduced about 0.15°C , but increases by about 0.15°C below 2000 m. However, as the GMR diffusivity increases from 1000 to 2000, the penetration of surface warming becomes shallower, with warming only occurring above 3130 rather than 3360 m due to relatively weaker MOTC. Therefore, the warming in the upper ocean above 1000 m is enhanced about 0.2°C , but reduced about 0.2°C below 1000 m. These changes in the vertical distribution of heating also contribute to the insensitivity of the total OHU.

The circulation anomaly in the North Atlantic is also changed (by 4–5 Sv) when different GMR diffusivities are applied. This appears to be associated with the difference of the warming pattern in the Atlantic. But readers should be cautious, since our diagnosis involves the difference of small anomalies. Power and Hirst (1997) proposed to separate the OHU into passive and dynamic components, which might help to diagnose the mechanisms of OHU. Further study of the uncertainty of convection parameterization is desirable, since it has a very important impact on the OHU as shown in our present study. These uncertainties of OHU will largely affect the rate of global warming that will take place as a result of increases in greenhouse gases, since the warming of the atmosphere depends on how rapidly the heating penetrates into the deep ocean.

Acknowledgments. The authors appreciate the comments from Dr. Ronald J. Stouffer and an anonymous reviewer. These comments helped to improve this manuscript.

REFERENCES

- Barnett, T. P., D. W. Pierce, and R. Schnur, 2001: Detection of anthropogenic climate change in the world's oceans. *Science*, **292**, 270–274.
- Boville, B. A., and P. R. Gent, 1998: The NCAR Climate System Model, version one. *J. Climate*, **11**, 1115–1130.
- Colman, R. A., S. B. Power, B. J. MacAvaney, and R. R. Dahni, 1995: A non-flux-corrected transient CO_2 experiment using the BMRC coupled atmosphere/ocean GCM. *Geophys. Res. Lett.*, **22**, 3047–3050.
- Cox, M. D., and K. Bryan, 1984: A numerical model of the ventilated thermocline. *J. Phys. Oceanogr.*, **14**, 674–687.

- Cubasch, U., K. Hasselmann, H. Hock, E. Maier-Reimer, U. Mikolajewicz, B. D. Santer, and R. Sausen, 1992: Time-dependent greenhouse warming computations with a coupled ocean-atmosphere model. *Climate Dyn.*, **8**, 55–69.
- Gent, P. R., and J. C. McWilliams, 1990: Isopycnal mixing in ocean circulation models. *J. Phys. Oceanogr.*, **20**, 150–155.
- Gregory, J. M., 2000: Vertical heat transports in the ocean and their effect on time-dependent climate change. *Climate Dyn.*, **16**, 501–515.
- Guo, Y., Y. Yu, X. Liu, and X. Zhang, 2001: Simulation of climate change induced by CO₂ increasing for East Asia with IAP/LASG GOALS model. *Adv. Atmos. Sci.*, **18**, 53–66.
- Hirst, A., and W. Cai, 1994: Sensitivity of a World Ocean GCM to changes in subsurface mixing parameterization. *J. Phys. Oceanogr.*, **24**, 1256–1279.
- Houghton, J. T., Y. Ding, D. J. Griggs, M. Noguer, P. J. van der Linden, and D. Xiaosu, Eds., 2001: *Climate Change 2001: The Scientific Basis*. Cambridge University Press, 944 pp.
- Huang, B., P. H. Stone, and C. Hill, 2003a: Sensitivities of deep-ocean heat uptake and heat content to surface fluxes and subgrid-scale parameters in an OGCM with idealized geometry. *J. Geophys. Res.*, **108**, 3015, doi:10.1029/2001JC001218.
- , —, A. P. Sokolov, and I. V. Kamenkovich, 2003b: The deep-ocean heat uptake in transient climate change. *J. Climate*, **16**, 1352–1363.
- Jenkins, W. J., 1991: Determination of isopycnal diffusivity in the Sargasso Sea. *J. Phys. Oceanogr.*, **21**, 1058–1061.
- Johns, T. C., R. E. Carnell, J. F. Crossley, J. M. Gregory, J. F. B. Mitchell, C. A. Senior, S. F. B. Tett, and R. A. Wood, 1997: The second Hadley Centre coupled ocean-atmosphere GCM: Model description, spinup and validation. *Climate Dyn.*, **13**, 103–134.
- Kamenkovich, I. V., A. P. Sokolov, and P. H. Stone, 2002: An efficient climate model with a 3D ocean and statistical-dynamical atmosphere. *Climate Dyn.*, **19**, 585–598.
- Ku, T. L., and S. Luo, 1994: New appraisal of Radium 226 as a large-scale oceanic mixing tracer. *J. Geophys. Res.*, **99**, 10 255–10 273.
- Ledwell, J. R., A. J. Watson, and C. S. Law, 1998: Mixing of a tracer in the pycnocline. *J. Geophys. Res.*, **103**, 21 499–21 529.
- , E. T. Montgomery, K. L. Polzin, L. C. St. Laurent, R. W. Schmitt, and J. M. Toole, 2000: Evidence for enhanced mixing over rough topography in the abyssal ocean. *Nature*, **403**, 179–182.
- Levitus, S., J. I. Antonov, T. P. Boyer, and C. Stephens, 2000: Warming of the world ocean. *Science*, **287**, 2225–2229.
- , —, J. Wang, T. L. Delworth, K. W. Dixon, and A. J. Broccoli, 2001: Anthropogenic warming of earth's climate system. *Science*, **292**, 267–270.
- Manabe, S., and R. J. Stouffer, 1994: Multiple century response of a coupled ocean-atmosphere model to an increase of atmospheric carbon dioxide. *J. Climate*, **7**, 5–23.
- , —, M. J. Spelman, and K. Bryan, 1991: Transient responses of a coupled ocean-atmosphere model to gradual changes of atmospheric CO₂. Part I: Annual mean response. *J. Climate*, **4**, 785–818.
- Marshall, J., A. Adcroft, C. Hill, L. Perelman, and C. Heisey, 1997: A finite volume, incompressible Navier stokes model for studies of the ocean on parallel computers. *J. Geophys. Res.*, **102**, 5753–5766.
- Meehl, G. A., W. D. Collins, B. A. Boville, J. T. Kiehl, T. M. L. Wigley, and J. M. Arblaster, 2000: Response of the NCAR climate system model to increased CO₂ and the role of physical processes. *J. Climate*, **13**, 1879–1898.
- Murphy, J. M., and J. F. B. Mitchell, 1995: Transient response of the Hadley Centre coupled ocean-atmosphere model to increasing carbon dioxide. Part II: Spatial and temporal structure of response. *J. Climate*, **8**, 57–80.
- Nakamura, M., and Y. Cao, 2000: On the eddy isopycnal thickness diffusivity of the Gent-McWilliams subgrid mixing parameterization. *J. Climate*, **13**, 502–510.
- Power, S. B., and A. C. Hirst, 1997: Eddy parameterization and oceanic response to idealized global warming. *Climate Dyn.*, **13**, 417–428.
- , R. A. Colman, B. J. McAvaney, R. R. Dahni, A. M. Moore, and N. R. Smith, 1993: The BMRC Coupled atmosphere/ocean/sea-ice model. BMRC Research-Rep. 37, Bureau of Meteorology Research Centre, Melbourne, Australia, 58 pp.
- Redi, M. H., 1982: Oceanic isopycnal mixing by coordinate rotation. *J. Phys. Oceanogr.*, **12**, 1154–1158.
- Russell, G. L., and D. Rind, 1999: Response to CO₂ transient increase in GISS coupled models: Regional coolings in a warming climate. *J. Climate*, **12**, 531–539.
- , J. R. Miller, and D. Rind, 1995: A coupled atmosphere-ocean model for transient climate change studies. *Atmos.-Ocean*, **33**, 683–730.
- Sokolov, A. P., and P. H. Stone, 1998: A flexible climate model for use in integrated assessments. *Climate Dyn.*, **14**, 291–303.
- Stouffer, R. J., and S. Manabe, 1999: Response of a coupled ocean-atmosphere model to increasing atmospheric carbon dioxide: Sensitivity to the rate of increase. *J. Climate*, **12**, 2224–2236.
- Thiele, G., 1986: Baroclinic flow and transient-tracer fields in the Canary-Cape Verde Basin. *J. Phys. Oceanogr.*, **16**, 814–826.
- Voss, R., R. Sausen, and U. Cubasch, 1998: Periodically synchronously coupled integrations with the atmosphere-ocean general circulation model ECHAM3/LSG. *Climate Dyn.*, **14**, 249–266.
- Wiebe, E. C., and A. J. Weaver, 1999: On the sensitivity of global warming experiments to the parameterisation of sub-grid scale ocean mixing. *Climate Dyn.*, **15**, 875–893.
- Zhang, H. M., M. D. Prater, and T. Rossby, 2001: Isopycnal Lagrangian statistics from North Atlantic Current RAFOS float observations. *J. Geophys. Res.*, **106**, 13 817–13 836.
- Zhang, X.-H., G.-Y. Shi, H. Liu, and Y.-Q. Yu, Eds., 2000: *IAP Global Atmosphere-Land System Model*. Science Press, 259 pp.